Identification and Interpretation of Representative Ozone Distributions in Association with the Sea Breeze from Different Synoptic Winds over the Coastal Urban Area in Korea

Mi-Kyoung Hwang and Yoo-Keun Kim
Division of Earth Environmental System, Busan National University, Busan, South Korea

In-Bo Oh
Institute for Multi-Dimensional Air Quality Studies, University of Houston, Houston, TX

Hwa Woon Lee and Cheol-Hee Kim
Division of Earth Environmental System, Busan National University, Busan, South Korea

ABSTRACT

To aid the studies of long-term impact assessment of cumulative ozone (O_3) exposures, the representative 8-hr O_3 pollution patterns have been identified over the Greater Seoul Area (GSA) in Korea. Principal component analysis and two-stage clustering techniques were used to identify the representative O_3 patterns, and numerical and observational analyses were also used to interpret the identified horizontal distribution patterns. The results yielded three major O_3 distribution patterns, and each of the three patterns was found to have strong correlations with local and synoptic meteorological conditions over the GSA. For example, pattern 1, accounting for 46% of O_3 concentration distributions, mostly occurred under relatively weak westerly synoptic winds. The predominant features of this pattern were infrequent high O_3 levels but a distinct gradient of O_3 concentration from the western coastal area to the eastern inland area that was mainly induced by the local sea breeze. Pattern 2, accounting for 31% of O_3 concentration distributions, was found with higher O_3 levels in the western coastal area but lower in the eastern inland area. This is due to the modified sea breeze under the relatively stronger easterly opposing synoptic wind, affecting the high O_3 occurrence in the western coastal area only. However, pattern 3, accounting for 21% of O_3 concentration distributions, showed significantly higher O_3 concentrations over the whole GSA mainly due to the retarded and slow-moving sea-breeze front under the weak opposing synoptic flow. Modeling study also indicated that local and synoptic meteorological processes play a major role in determining the high O_3 concentration distribution patterns over the GSA.

INTRODUCTION

Ground-level ozone (O_3) adversely affects vegetation and human health.[1] In assessing plant response and health effects, the duration of exposure as well as peak concentration of O_3 has been recognized to be an important factor.[1–4] In 1997, the U.S. Environmental Protection Agency (EPA) promulgated a new 8-hr standard for estimating multiple-hour exposures to moderate O_3 concentrations, and the 8-hr standard has been used in several impact assessments using data analysis and modeling studies.[5–8] Multiyear photochemical model simulation is the most promising way to address the cumulative O_3 exposure problem, done through precise, long-term impact studies of high O_3 concentrations. However, running air quality models that cover longer-periods have generally been prohibitively complicated because of incomplete emission inventories and difficulties in constructing precise wind fields. Numerical modeling studies have suggested that, because of input demand and computational load, an episode aggregation approach by identifying several representative air quality patterns is an effective alternative to developing and running a long-term air quality model. For this reason, the air quality regimes over non-urban areas utilizing the spatiotemporal variability of daily maximum 8-hr O_3 concentrations have been classified.[9]

Measurement studies have shown that the spatiotemporal variability of daily maximum 8-hr O_3 patterns over coastal areas vary considerably due to the accumulation and transport of O_3 by meteorological effects (i.e., land/sea-breeze circulation), requiring adequate quantitative photochemical as well as meteorological observations.[10–14] For example, in the San Francisco and Monterey Bay

IMPLICATIONS

The GSA in South Korea has experienced the serious O_3 problem caused by dense population and industrial actives. This paper focused on the episodic aggregation approaches for study cumulative O_3 exposures over GSA by deriving the various spatial patterns of 8-h O_3 concentration using statistical analysis, and also understanding the dynamic effects of meteorology on each pollution pattern. The quantitative interpretation associated with patterns may attribute to environment assessment for long-term as well as improvement for prediction capability of O_3 over the GSA.

areas, although the spatial patterns of daily maximum 1-hr O_3 concentration had been defined,[15] the characteristics of O_3 patterns in association with meteorological conditions were not substantiated because of the limitations on the number of coastal sites. Lehman et al.[9] suggests that future work should involve an investigation of the dependence of O_3 concentrations on meteorology for identifying O_3 distribution patterns. More recently, it was shown that the timing and penetration of the sea breeze coupled with synoptic forces can play an important role in determining high O_3 concentration distributions.[14,16,17] However, limited episodes focusing on short-term O_3 exposures have been examined, and consequently the representative O_3 patterns for long time periods have not been quantitatively elucidated.

The purpose of this paper is to identify representative spatial O_3 distribution patterns on the basis of a quantitative statistical analysis of multi-year daily maximum 8-hr O_3 measurements to aid in assessing cumulative O_3 exposures over coastal urban areas in the Greater Seoul Area (GSA) in South Korea. Interpretations of the local circulation and synoptic conditions are attempted to explain the identified representative spatial O_3 distribution patterns. As a case study, the meteorological effect on O_3 level in each representative pattern was also simulated by using the MM5 (Meteorological Model generation 5; Pennsylvania State University/ National Center for Atmospheric Research [PSU/ NCAR] Mesoscale Modeling System).

METHODOLOGY
Geographical Features in the GSA and Data
The GSA in South Korea comprises Seoul, the capital of South Korea, and its neighboring satellite cities (Figure 1).

It has an area of approximately 7000 km² with 22.1 million inhabitants, accounting for approximately 45% of the total population of South Korea. Seoul, together with the industrial cities located near the western coastline, are the predominated emission sources of O_3 precursors (oxides of nitrogen [NO_x], volatile organic compounds), resulting in a steadily increasing tend of ambient O_3 concentrations since the early 1990s.[18] The GSA is mostly surrounded by many mountains in the east and the Yellow Sea in the west, where complex local circulations occur. The sea breeze is modified by channeling through valleys and is blocked by mountains.

The O_3 data used in this study were the measured daily maximum 8-hr concentrations from 54 sites (Figure 2) obtained from April to September over 7 yr (1998–2004). Hourly O_3 concentrations were measured at approximately 7–15 m above ground level using an ultraviolet (UV) photometric absorption method. By taking the moving average, the 8-hr O_3 concentrations were calculated from hourly O_3 values at each site, and on a daily basis, daily maximum 8-hr O_3 concentrations were determined. As a consequence, the daily maximum 8-hr O_3 that exceeded the air quality standard of 80 parts per billion (ppb) was used. The result yielded 180 days (episodes) for this study.

Hourly meteorological data were also used. The meteorological data were gathered from 48 observation sites in total: 46 sites of Automatic Weather System (AWS, which is the automated version of the Surface Weather Observation System) and 2 specific sites labeled the Seoul weather station (SWS) and the Incheon International Airport weather station (IWS). In this study SWS (located in an inland urban area) and IWS (located in a western
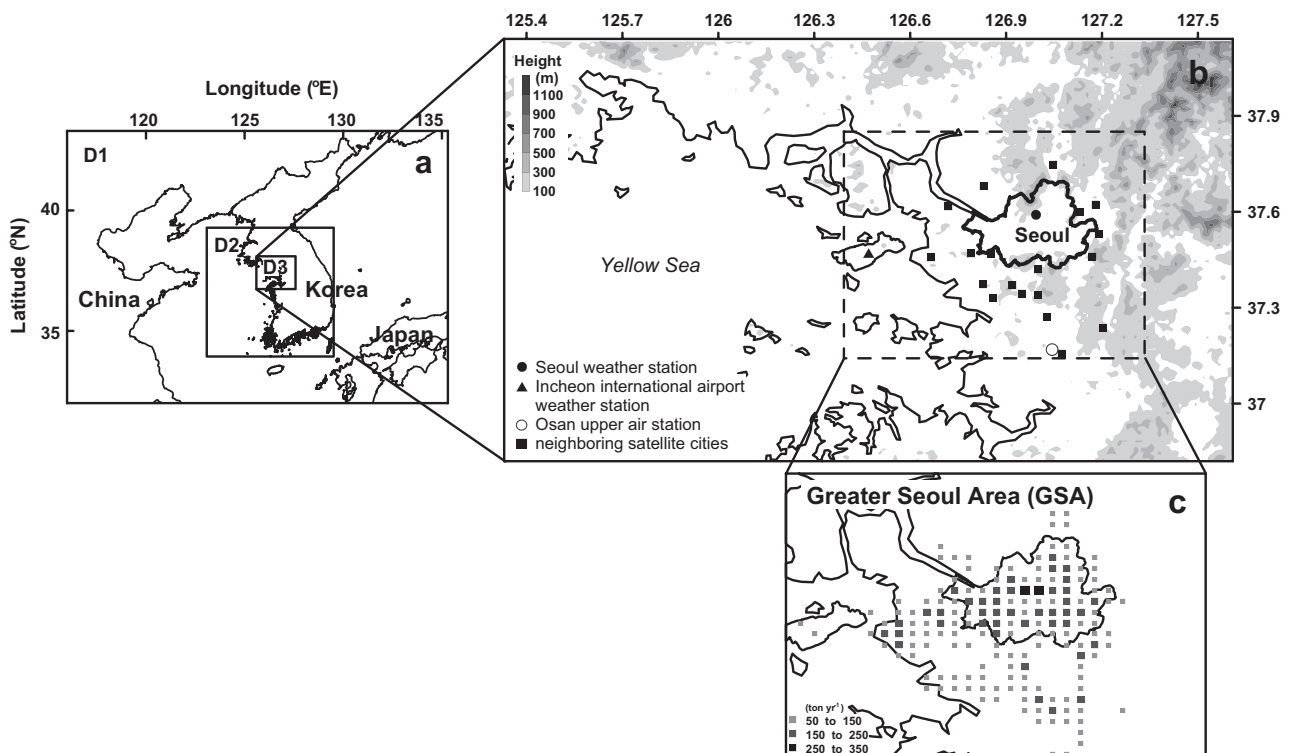
Figure 1. (a) Three-level nested domain of MM5 model, (b) the terrain height for the magnified domain 3 and the location of meteorological stations and satellite cites near Seoul, and (c) NO_x emissions with the 3-km resolution in the GSA.
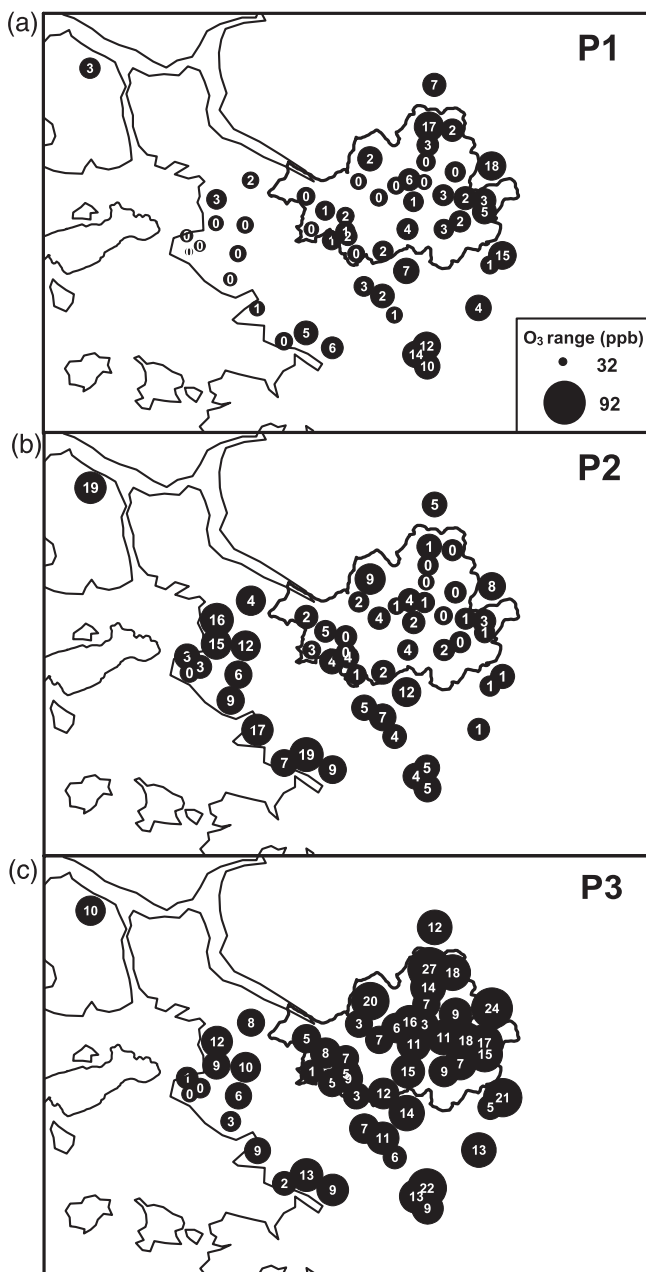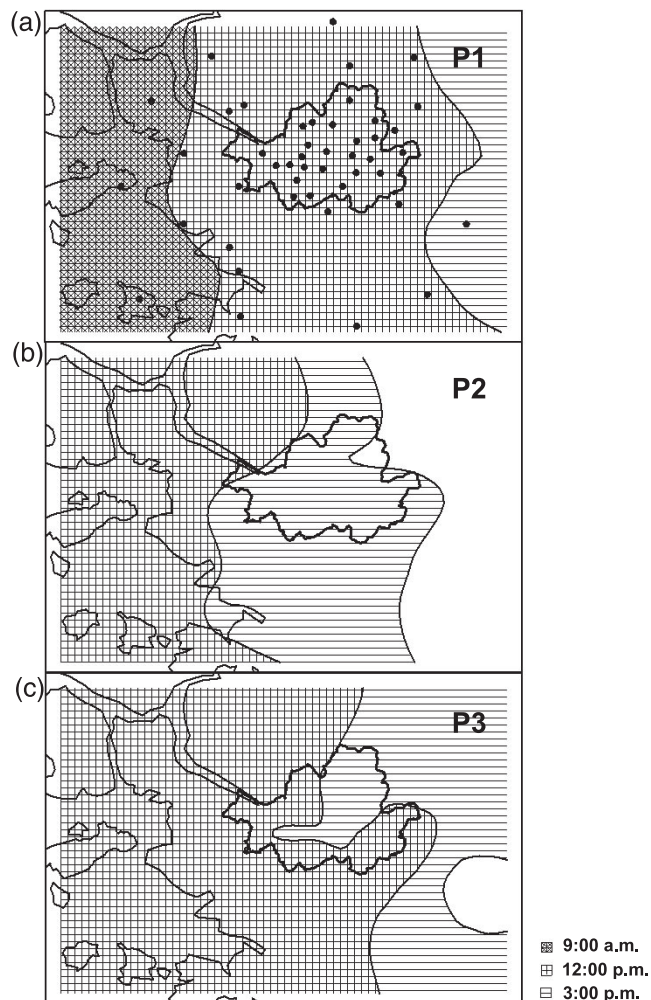
Figure 2. Horizontal distributions of the average daily maximum 8-hr O_3 concentrations (dark circles) and the number of days exceeding the 8-hr standard (numbers within the circles) for each of the three O_3 patterns (a) P1, (b) P2, and (c) P3 over the GSA.

coastal suburban area) were both used to examine the meteorological conditions associated with O_3 distribution. All of the locations of the meteorological sites are denoted in Figures 1 and 3. All of the meteorological data were obtained at an altitude of approximately 10 m above ground level. In addition, the vertical wind profiles (observed twice a day) obtained at the Osan upper air station (denoted in Figure 1b) were used to identify the synoptic flow. The instruments used for both the O_3 measurements and meteorological observations used in this study were regularly calibrated by the Korea Ministry of Environment and the Korea Meteorological Administration (KMA), respectively.

Principal Component Analysis and Cluster Analysis

In this study, a three-step process consisting of principal component analysis (PCA) and two-stage cluster analysis techniques were used to identify O_3 distribution patterns. Before the two-stage cluster analysis, PCA was used. As Eder et al.[19] described earlier, the central idea of PCA is to reduce the dimensionality of a voluminous dataset consisting of a large number of interrelated input dataset of 8-hr O_3 concentrations to explain variance. Here, the size of the dataset has been reduced, and the original data matrix was reconstructed into principal components in which most of the essential information was explainable by retaining the first few principal components.[20,21] In this study, the daily maximum 8-hr O_3 concentrations obtained at each of the 54 sites for the 180 episodes were formulated into the original matrix having a total original dimension of (180 episodes $\times$ 54 sites = 9720 observations). In formulating the matrix, the missing values were replaced by the nearest sites using a linear interpolation method. To decompose the O_3 pattern more clearly, a weighting technique in the PCA procedure was applied.

Figure 3. Horizontal distributions of the positive u-wind components (westerly) observed at 46 AWS (black dots) at 9:00 a.m. LST, 12:00 p.m. LST, and 3:00 p.m. LST for each of the three O_3 patterns (a) P1, (b) P2, and (c) P3 over the GSA.

This weighting technique was used to produce a statistically more distinctive decomposition by relatively weighting the each observation in the input dataset.[21,22] In this study, the number of sites exceeding the 8-hr standard was enumerated for each episode and used as a weighting factor for all of individual observations in PCA procedure. As a result, only the first few principal components that explain a large amount of the total variation have been derived. The appropriate number of principal components that were retained was approximated using the Screen test.[23]

Derived from the principal components, both the hierarchical and nonhierarchical algorithms were employed as two-stage clustering techniques. As a first stage, the average linkage, which is also called a hierarchical agglomerative method, is used to determine the number of clusters in advance on the basis of the statistical indices of R^2, Pseudo-F, and Pseudo-t^2. As a second stage, the initial clusters classified by average linkage are then refined by using the K-means, which provides the final solution. This two-stage algorithm was recommended because this combined approach is superior to a one-stage approach, such as only using the average linkage in terms of cluster cohesiveness.[19] More complete clustering algorithms are described by Eder et al.[19] and Davis et al.[24]

Configuration of MM5 Modeling

MM5 (version 3.6) was used to analyze wind fields to explain the meteorological conditions relevant to the O_3 patterns identified over the GSA. MM5 was set to use three nested grid domains: (1) the outermost domain (60×48 grid points) with a grid spacing of 27 km that covers northeast Asia, (2) the first nested domain (64×61 grid points) with a grid spacing of 9 km that covers the entire Korean peninsula, and (3) the second nested domain (67×49 grid points) with a grid spacing of 3 km that covers only the GSA, as shown in Figure 1. The vertical grid consists of 30 full-σ levels with higher spacing near the ground. The lowest layer above the ground is 30 m and the top is at 100 hPa. The initial and lateral boundary conditions were obtained from the Regional Data Assimilation and Prediction System (RDAPS) that has been provided by KMA.[25] RDAPS consists of 3-hr interval reanalysis meteorological fields.

On the basis of the multiscale nudging technique,[26] analysis nudging (nudging by gridded RDAPS data) was imposed on both the outermost domain and first nested domain, whereas observational nudging (nudging by observational data) was only imposed on the second nested domain. The nudging coefficient, G, was set to $2.5 \times 10^{-4} \cdot \text{sec}^{-1}$ for wind and temperature on the 27- and 9-km grid spacing domains, respectively, and $4 \times 10^{-4} \cdot$ sec^{-1} for wind on the 3-km grid. The microphysical schemes that were used were the rapid radiative transfer model (RRTM) for radiation schemes, the Grell scheme for cumulus parameterization (only used on the 27-km grid domain), and the medium range forecast (MRF) for planetary boundary layer (PBL) schemes. The model simulation was performed for 6 days from 9:00 a.m. LST (Local Standard Time) on June 4 to 12:00 p.m. LST on June 9.

RESULTS AND DISCUSSION
Major Patterns of 8-hr O_3 Pollution

Table 1 shows the results of the Screen test[23] in the PCA procedure, suggesting that five principal components of a matrix (180×5) could explain 70.7% of the total variance. That result suggests that by retaining only the first five principal components, a large amount of the original O_3 concentration variations were explained. On the basis of these principal components, the hierarchical and nonhierarchical algorithms were both used as a two-stage clustering technique.

Table 2 summarizes the results of the average linkage analysis (hierarchical stage) from which an initial number of clusters was determined before the application of K-mean (nonhierarchical stage). In accordance with the technical guideline of cluster analysis, the number of clusters was selected from a guide at the time when both pseudo-F and pseudo-t^2 were maximal, with the largest drop in R^2 as the number of clusters decreased[20] (denoted in boldface in Table 2). Given the results in Table 2, four clusters were selected and were used as input parameters to formulate the K-mean clustering. This result indicates that the original 180 episodes in total were finally grouped into four clusters. As a next and final step, the K-mean analysis was used to refine and generate the final cluster solution. The K-mean analysis used here is the iterative approach that allows all of the episodes to reclassify even after they have been grouped into the same cluster.

Table 3 shows the number of days and 8-hr O_3 statistics for each of the four identified clusters. However, as illustrated in Table 3, cluster 4 (C4) accounts for infrequent episodes because it contains only a few cases with relatively lower O_3 levels. Therefore in this study we considered only three clusters (C1, C2, and C3) as representatives occupying approximately 98% (176 episodes) of the total episodes. Each of the three clusters was identified to retain noticeable differences in the characteristics of observed O_3 concentrations such as O_3 levels, distribution patterns, and number of stations exceeding standard

Table 1. Statistics for first five principal components.

	PC 1	PC 2	PC 3	PC 4	PC 5
Eigenvalue	20.15	8.65	4.93	2.49	1.96
Explained variance (%)	37.31	16.02	9.14	4.62	3.62
Cumulative explained variance (%)	37.31	53.33	62.47	67.09	70.71

Table 2. Statistical tests for determining number of clusters to retain.

Number of clusters	Pseudo-F	Pseudo-t^2	R^2
6	24.72	6.11	0.41
5	27.47	19.22	0.39
4	**35.32**	3.41	**0.38**
3	27.63	**39.24**	**0.23**
2	24.75	26.84	0.12
1	–	24.75	0.00

Table 3. Summary for statistics of the daily maximum 8-hr O_3 concentrations for different clusters.

Cluster	O_3 Pattern	Number of Days (%)	Average of the Daily Maximum 8-hr O_3 (ppb)	Number of Stations Exceeding 80 ppb/8 hr
C1	P1	83 (46.1)	53.3 ± 8.2	2.1 ± 1.9
C2	P2	56 (31.1)	59.9 ± 7.3	4.5 ± 4.8
C3	P3	37 (20.6)	70.8 ± 10.1	14.5 ± 8.8
C4	–	4 (2.2)	22.7 ± 7.4	1.0 ± 0.0

level. In association with the local and synoptic winds, these three clusters were used to interpret the meteorological impact on the representative O_3 distributions. Hereafter, clusters 1, 2, and 3 will be referred to as patterns 1, 2, and 3.

Figure 2 presents the horizontal distributions of the 8-hr O_3 levels and the frequency that exceeded the standard of 80 ppb for each of the three patterns. Pattern 1 (P1) accounted for approximately 46% of the total episodes and had a similar distribution pattern as the average O_3 distribution for special episodes related to the observed sea-breeze circulation under the westerly synoptic condition in the GSA.[18] In both the O_3 concentration and occurrence frequency exceeding the standard of 80 ppb, some gradient was found between the coastal region and the eastern inland area (Figure 2). Both the O_3 levels (53 ± 8.2 ppb) and number of sites exceeding the standard of 80 ppb (2.1 ± 1.9 sites) was lower than in other patterns (Table 2).

Pattern 2 (P2) accounted for 31.1% (56 episodes) of the total episodes and had a more frequent occurrence of higher O_3 concentrations than that of P1. This pattern particularly exhibited elevated O_3 concentrations over the western coastal area in comparison with P1, whereas exhibiting lower levels over the western inland area. Therefore, this is rather characterized by higher O_3 concentration in the western coastal area due to the convergence zone along the western coastal area formed by combining the sea breeze (westerly) and synoptic flow (easterly). Considering the relatively lower emission of O_3 precursors in the western coastal area, this pattern is most likely due to the impact of meteorological conditions such as surface easterly winds.

Pattern 3 (P3) accounted for 20.6% (37 episodes) of the total episodes, and had a similar pattern to P1, to some extent, except for the pollution level. It had significantly higher O_3 levels, reaching approximately 71 ppb on average, and severely exceeded the standard of 80 ppb (14.5 ± 8.8 sites) compared with the other two patterns. Most episodes belonging to this pattern occurred in stagnating synoptic conditions with slowly moving high-pressure systems or relatively weak easterly (or sometimes weak westerly) 850-hPa geostrophic winds over the GSA. When these synoptic conditions occur, other meteorological factors such as high temperatures, low wind speeds, and intense solar radiation, which are closely related to the high O_3-forming potentials also occur.
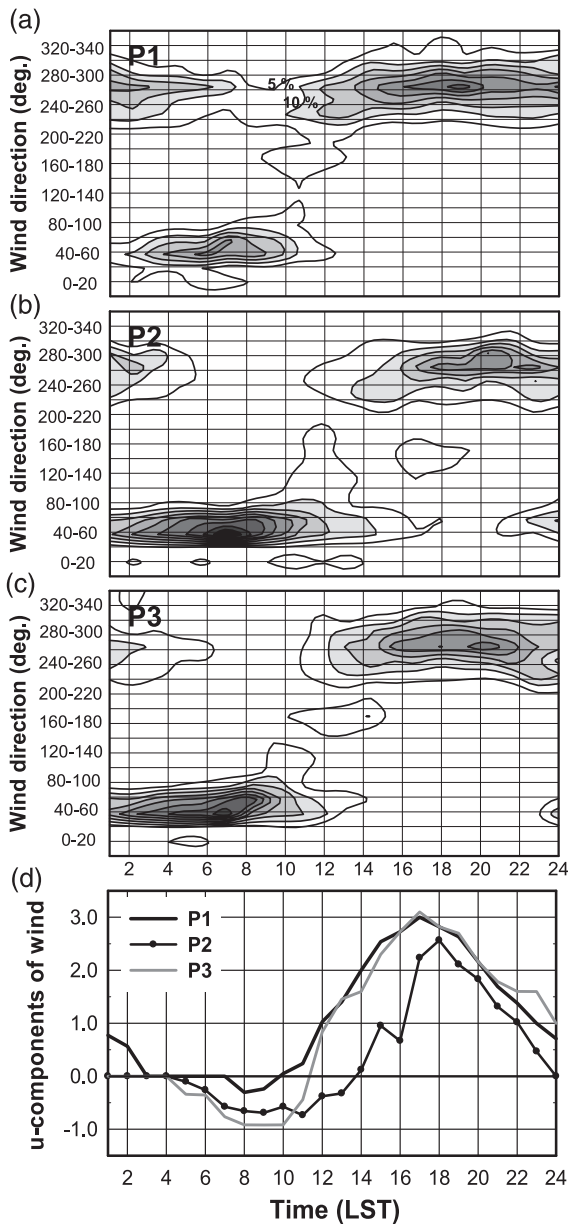
Association of the Sea Breeze Combined with Synoptic Flow

To examine the meteorological effects on the identified 8-hr O_3 concentration patterns, the correlation between O_3 concentrations and meteorological measurements, including both surface and upper air observations were analyzed. Because solar radiation and temperature are crucial factors in determining photochemical production, the measurements of these two meteorological factors in each identified pattern have been compared. Comparing these meteorological factors at both SWS and IWS demonstrated that no statistical differences of meteorological parameters among all three of the patterns had occurred. For example, in each of the three patterns, the daily maximum temperature and daily solar radiation at SWS were all more than 29 °C and 18.3 MJ · m^{-2} · day^{-1}, respectively. These conditions indicate that there have been no significant differences in the potential for photochemical O_3 production, thereby indicating that the dynamic and meteorological effects of the atmosphere could be more important for the different O_3 patterns, rather than the generation of O_3 from photochemical reactions.

This is more obvious in Figure 3, which shows the positive u-components of wind (westerly) at the 46 AWS observation sites at 9:00 a.m., 12:00 p.m., and 3:00 p.m. LST, respectively. The leading edge of the positive u-components (which resembles a sea-breeze front) was formed at different hours in each of the three patterns. The leading edge of the positive u-components in P1 started early, with high O_3 concentration over the eastern part of the GSA. It was found near the western coastline at 9:00 a.m. LST and arrived at Seoul at 12:00 p.m. LST in P1. However, P2 appears later than P1, with relatively higher O_3 concentrations over the western GSA. This suggests that the identified O_3 patterns were closely related to the onset of the sea-breeze front and its propagations, and therefore the wind fields in each of the three patterns derived by sea-breeze development and penetrations had great capabilities to explain the pattern of O_3 concentrations over the GSA.

Figure 4 shows the diurnal variation of wind direction as well as medians of the u-component at SWS, and Figure 5 presents the distributions of the u-components at 850 hPa at 9:00 a.m. LST obtained from the Osan upper air station in each of the three patterns. According to Figures 4 and 5, the diurnal variation of the winds was largely governed by the sea breeze in the morning together with a synoptic westerly flow that prevents the development of the sea breeze. For example, it should be noted for P1 that the obvious westerly sea breeze reached Seoul at around 10:00 a.m. LST induced by the westerly synoptic flow (Figure 3) with a low wind speed (57% for u-component ranging from 0 to 5 m · sec^{-1}). Therefore, with an onshore synoptic force such as that in Figure 5,

Figure 4. Diurnal variations of wind direction (%) for (a) P1, (b) P2, and (c) P3. (d) The u-component of wind at SWS for each of the three O$_3$ patterns (P1, P2, and P3). The positive u-component of wind is westerly.

until approximately 2:00 p.m. LST. These surface wind patterns indicate that there is a strong possibility that the development of the sea breeze was suppressed by synoptic forces,[31] although both P1 and P2 have similar inland surface temperatures. Figure 5 also shows the offshore synoptic flow frequently observed in P2 (68.7%), which all support the association of a sea breeze with an opposing synoptic flow giving rise to late sea breeze.

Ding et al.[16] have also shown that the sea breeze delayed by the offshore synoptic flow is an important factor in high concentrations of O$_3$ in coastal areas. The recirculation of polluted air originating from coastal source areas is also suggested in association with a late sea breeze,[17,32] which makes it possible for the O$_3$ levels along the coast to increase. In the same manner, O$_3$ levels over the western coastal area in P2 were found to increase similarly, due to the late sea breeze resulting from its interaction with the offshore synoptic flow. Thus, in this pattern, the prevailing easterly synoptic winds lasting until the early afternoon are well characterized by a high potential to enhance O$_3$ concentration patterns in the western GSA, as has been demonstrated in previous studies.

However, P3 shows a different O$_3$ pattern in Figure 3. Positive u-components reached Seoul at 12:00 p.m. LST and then moved eastward in the afternoon. The change to westerly components at SWS occurred earlier than P2 but later than P1, as shown in Figure 4, although the wind fields of P3 seem similar to P2. This similarity implies that O$_3$ and its precursors can accumulate over western GSA under the easterlies, with low wind speed (less than 2 m · sec^{-1} at SWS) during the morning. After midday, P3 became similar to P1 in the magnitude of the positive u-component, which means accumulated pollutants can be transported eastward when the photochemical production of O$_3$ was maximized by the optimal photochemical conditions. As a result, extremely high O$_3$ levels covering the entire GSA were found in this pattern (Figure 2).
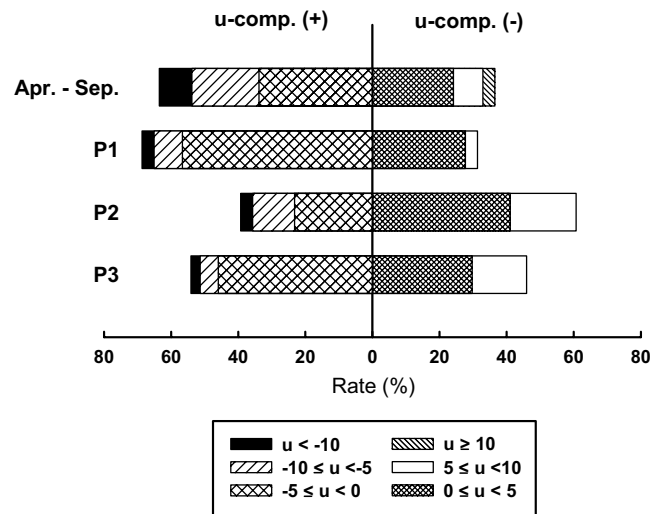
the sea-breeze development was initiated earlier and progressed over the GSA until evening.[27] Thus it is obvious that the polluted air over the western GSA was transported by the early sea breeze, and led to high O$_3$ concentrations over the eastern GSA where there are no heavy emission sources.[28–30] In this manner, the O$_3$ distributions with the distinct east-west gradient of O$_3$ in P1 were inseparably connected to the development of the sea breeze under the onshore synoptic flow.

On the contrary, P2 shows a rather different wind flow. The positive u-component was not found inland until 12:00 p.m. LST in P2 (Figure 3). Only after 12:00 p.m. LST did it gradually start to extend inland. In Figure 4, the diurnal variation of winds at SWS shows the retarded sea breeze when the easterly wind was prevalent

Figure 5. Occurrence frequency (%) of u-component at the 850-hPa level observed at the Osan upper air station at 9:00 a.m. LST for each of the three O$_3$ patterns (P1, P2, and P3). The positive u-component of wind is westerly.

A Case Study for Major O₃ Patterns

To verify the effects attributed to the sea breeze associated with each O₃ pattern, a numerical simulation using MM5 was performed for three typical cases (June 5, 8, and 9, 2003). During this period, each of the three identified O₃ patterns occurred with the substantiated change of both surface wind and synoptic flow. Both high daily maximum temperatures (29–31 °C) and strong solar radiation (23.2–23.5 MJ · m⁻² · day⁻¹) at SWS were observed.

Figure 6, a–c, shows the maximum 8-hr O₃ concentrations observed at air monitoring sites as well as the simulated surface wind fields with sea-breeze front lines at 3:00 p.m. LST. Figure 6, d–f, shows the longitude-time cross-section for u-components of simulated surface wind and wind speed. The cross-section was taken over the latitude of 37.6 °E across the center of Seoul. The simulated horizontal wind fields (not shown) reproduce diurnal variations in winds with reasonable accuracy. For example, the simulations at SWS have a minor discrepancy from observations in wind direction and speed with a root mean square error of 19° and 0.5 m · sec⁻¹ on average, respectively.

On June 5, relatively higher O₃ concentrations were observed in the eastern and southern part of the GSA. Four monitoring sites (shaded circles) reported high O₃ levels exceeding 80 ppb/8 hr, as illustrated in Figure 6a. Under a high pressure system located over the Yellow Sea, north-westerly synoptic flow enhanced the surface westerly (positive u-component)[33] after 0900 LST and then rapidly penetrated further inland (Figure 6d) causing dominant westerly surface winds of 4 m sec⁻¹ over the entire GSA at 3:00 p.m. LST. These wind fields made the quick transportation of the pollutants emitted at the western coastal area in the morning possible causing relatively higher 8-hr O₃ concentrations on the eastern part of the GSA.[11,29,30] This feature is well characterized in P1, as described in the previous section.

On the following 2 days (June 6 and 7), there were no interesting distributions of O₃ concentrations because of little precipitation and low temperatures. However, on
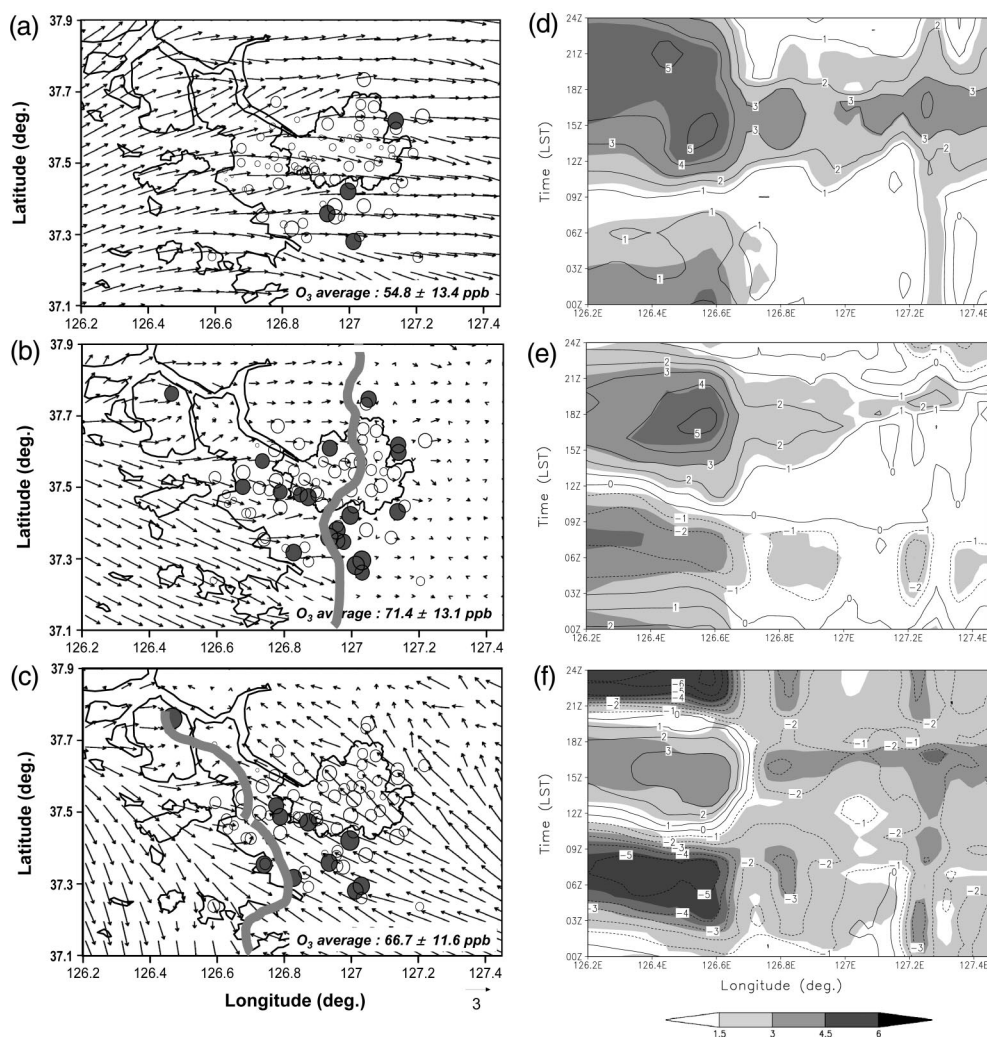
Figure 6. Simulated horizontal wind fields at 10 m above ground level at 3:00 p.m. LST, with the observed daily maximum 8-hr O₃ concentrations (left panels), and longitude-time cross-section of u-wind components (shaded area denotes wind speed in m · sec⁻¹) along the latitude of 37.6° (right panels) on June 5 (a and d), June 6 (b and e), and June 9 (c and f) in 2003. The size of circles in left panels indicates the average concentrations varying from 30 to 120 ppb. Shaded circles and thick shaded lines in the left panels indicate the sites exceeding the 8-hr O₃ standard and the location of the sea-breeze front estimated from the convergence of winds, respectively.

the next day (June 8), very high concentrations (average: 71.7 ± 13.2 ppb/8 hr) were observed throughout the GSA and O_3 exceeding 80 ppb occurred at 20 sites, with a maximum 8-hr O_3 concentration of 96.5 ppb (Figure 6b). The synoptic features showed that, as the North Pacific High gradually expanded toward the Korean peninsula, the weak southeasterly flow (~5 m $\cdot$ sec^{-1} at the Osan upper air station) prevailed at the 850-hPa level on that day. This pattern well represents P3. Furthermore, low wind speed (i.e., <1.5 m $\cdot$ sec^{-1}) was simulated inland in the morning due to its influence on offshore flow (Figure 6e). This implies that these local and synoptic meteorological conditions contributed to the high accumulation of O_3 and its precursor over the entire GSA. The positive u-component slowly expanded inland after 11:00 a.m. LST and was near Seoul's center (127 °E) at 3:00 p.m. LST. Because the slowly moving sea breeze transported it, much higher O_3 concentrations could occur in the downstream area rather than in the high emission areas. In addition, on the basis of potential temperatures observed over Seoul during June 6–9, significant increases in O_3 concentrations occurred, in part because of the lower mixing height (~1.5 km) at 3:00 p.m. LST than that of other days,[34] which led to a weak dilution of the primary emissions within the mixing layer.[35,36]

On June 9, a southeasterly synoptic flow was strengthened by an increasing pressure gradient under the North Pacific High (~10 m $\cdot$ sec^{-1} on an 850-hPa level over the Korean peninsula). The O_3 level rapidly decreased (average: 66.9 ± 11.6 ppb/8 hr) with only nine sites in the southwestern GSA area exceeding the 8-hr standard (Figure 6c). It is clear that the positive u-components with calm conditions (<1.5 m $\cdot$ sec^{-1}) were at shoreline after midday but did not extend further inland during the day, as shown in Figure 6f. This condition corresponds to P2, in which O_3 levels in the western GSA were influenced by the transport of pollutants from inland high emission areas. Thus, the recirculation of air loaded with O_3 or its precursors frequently occurred with the late sea breeze, apparently leading to higher O_3 concentrations in the coastal GSA area.[17,31,37]

CONCLUSIONS

It is generally believed that multiyear simulation of a photochemical simulation of a photochemical model is needed because O_3 standards for protecting crops and other vegetation are assessed ideally on the basis of cumulative O_3 exposures. For this purpose the identification of the cumulative observed O_3 statistics was attempted over the coastal GSA. Also, numerical and observational analyses were applied to interpret the dependency of identified horizontal surface 8-hr O_3 pollution distribution patterns on meteorological variables.

By employing the PCA and two-stage clustering techniques on the basis of a daily maximum 8-hr O_3 concentration for a 7-yr period from 1998 to 2004, three major patterns of surface 8-hr O_3 pollution distribution were identified. Each pattern showed a different horizontal gradient and level of O_3 concentration, with a strong correlation with the transport and the accumulation of pollutants under the different meteorological conditions. In particular, the measurements of surface/upper wind

fields showed the different ranges and timing of sea-breeze penetration due to the different synoptic flows and played an important role in determining the 8-hr O_3 patterns. In a case study of three typical days, the effects of the early and late developing sea breeze under onshore and offshore synoptic flow were reconfirmed. These synoptic flows had the behavior of pollutants, resulting in quite different patterns of daily maximum 8-hr O_3 concentrations. Through this study, an emphasis was also put on the role of meteorological or dynamic processes that control O_3 distributions over a coastal urban area. For example, three 8-hr O_3 pollution patterns were clearly identified by unique meteorological and synoptic conditions. Therefore, their associations with the development of sea breezes under the different synoptic winds were able to be well substantiated by the characteristics of typical high O_3 concentration episodes.

In this study, we derived statistical daily maximum 8-hr O_3 concentration patterns representing real meteorological conditions. These representative patterns were found to be consistent with the characteristics of a typical episode in Korea. They will be used to quantify longer-term O_3 exposures, to assess their impact, or to generate estimates for protecting human health and vegetation in the GSA. In addition, detailed photochemical modeling approaches covering multiyear simulations will be tested to further confirm the reliability of the results derived in this study.

REFERENCES

1. *Air Quality Criteria for Ozone and Related Photochemical Oxidants, Vol. I*; EPA-600/R-05/004aF; U.S. Environmental Protection Agency: Research Triangle Park, NC, 2006.
2. Pedersen, U.; Lefohn, A.S. Characterizing Surface Ozone Concentrations in Norway; *Atmos. Environ.* **1994**, *28*, 89-101.
3. Lefohn, A.S.; Laurence, J.A.; Kohut, R.J. A Comparison of Indices that Describe the Relationship between Exposure to Ozone and Reduction in the Yield of Agricultural Crops; *Atmos. Environ.* **1988**, *22*, 1229-1240.
4. McDonnell, W.F.; Abbey, D.E.; Nishino, N.; Lebowitz, M.D. Long-Term Ambient Ozone Concentration and the Incidence of Asthma in Nonsmoking Adults: the Ahsmog Study; *Environ. Res.* **1999**, *80,* 110-121.
5. Chock, D.P.; Chang, T.Y.; Winkler, S.L.; Nance, B.I. The Impact of an 8-hr Ozone Air Quality Standard on ROG and NO_x Controls in Southern California; *Atmos. Environ.* **1999**, *33*, 2471-2485.
6. Lehohn, A.S.; Shadwick, D.S.; Ziman, S.D. The Difficult Challenge of Attaining EPA's New Ozone Standard; *Environ. Sci. Technol.* **1998**, *32*, 276-282.
7. Reynolds, S.D.; Blanchard, C.L.; Ziman, S.D. Understanding the Effectiveness of Precursor Reductions in Lowering 8-hr Ozone Concentrations—Part II. The Eastern United States; *J. Air & Waste Manage. Assoc.* **2004**, *54*, 1452-1470.
8. Sistla, G.; Hogrefe, C.; Hao, W.; Ku, J.-Y.; Zalewsky, E.; Henry, R.F.; Civerolo, K. An Operational Assessment of the Application of the Relative Reduction Factors in the Demonstration of Attainment of the 8-hr Ozone National Ambient Air Quality Standard; *J. Air & Waste Manage. Assoc.* **2004**, *54*, 950-959.
9. Lehman, J.; Swinton, K.; Bortnick, S.; Hamilton, C.; Baldridge, E.; Eder, B.; Cox, B. Spatio-Temporal Characterization of Tropospheric Ozone across the Eastern United States; *Atmos. Environ.* **2004**, *38*, 4357-4369.
10. Lalas, D.P.; Tombrou-Tsella, M.; Petrakis, M.; Asimakopoulos, D.N.; Helmis, C. An Experimental Study of the Horizontal and Vertical Distribution of Ozone over Athens; *Atmos. Environ.* **1987**, *21*, 2681-2693.
11. Liu, H.; Chan, J.C.L. An Investigation of Air-Pollutant Patterns under Sea-Land Breezes during a Severe Air-Pollution Episode in Hong Kong; *Atmos. Environ.* **2002**, *36*, 519-601.
12. Liu, K.-Y; Wang, Z.; Hsiao, L.-F. A Modeling of the Sea Breeze and its Impacts on Ozone Distribution in Northern Taiwan; *Environ. Model. Software* **2002**, *17*, 21-27.
13. Ghim, Y.S.; Oh, H.S.; Chang, Y.S. Meteorological Effects on the Evolution of High Ozone Episodes in the Greater Seoul Area; *J. Air & Waste Manage. Assoc.* **1995**, *51*, 185-202.

14. Ma, Y.; Lyons, T.J. Recirculation of Coastal Urban Air Pollution under a Synoptic Scale Thermal Trough in Perth, Western Australia; *Atmos. Environ.* **2003**, *37*, 443-454.
15. Ludwig, F.L.; Jiang, J.-Y.; Chen, J. Classification of Ozone and Weather Patterns Associated with High Ozone Concentration in the San Francisco and Monterey Bay Areas; *Atmos. Environ.* **1995**, *29*, 2915-2928.
16. Ding, A.; Wang, T.; Zhao, M.; Wang, T.; Li, Z. Simulation of Sea-Land Breezes and a Discussion of Their Implications on the Transport of Air Pollution during a Multi-Day Ozone Episode in the Pearl River Delta of China; *Atmos. Environ.* **2004**, *38*, 6737-6750.
17. Oh, I.-B.; Kim, Y.-K.; Lee, H.W.; Kim, C.-H. An Observational and Numerical Study of the Effects of the Late Sea Breeze on Ozone Distributions in the Busan Metropolitan Area, Korea; *Atmos. Environ.* **2006**, *40*, 1284-1298.
18. Ghim, Y.S.; Chang, Y.S. Characteristics of Ground-Level Ozone Distributions in Korea for the Period of 1990–1995; *J. Geophys. Res.* **2000**, *105*, 8877-8890.
19. Eder, B.K.; Davis, J.M.; Bloomfield, P. An Automated Classification Scheme Designed to Better Elucidate the Dependence of Ozone on Meteorology; *J. Appl. Meteorol.* **1994**, *33*, 1182-1199.
20. Eder, B.K.; Davis, J.M.; Bloomfield, P. A Characterization of the Spatiotemporal Variability of Non-Urban Ozone Concentrations over the Eastern United States; *Atmos. Environ.* **1993**, *27A*, 2645-2668.
21. Jolliffe, I.T. *Principal Component Analysis*, 2nd ed.; Springer: New York, 2002; pp 382-385.
22. *SAS/STAT User's Guide,* Version 8; SAS Institute: Cary, NC, 1999.
23. Cattell, R.B. The Screen Test for the Number of Factors; *Multivariate Behav. Res.* **1966**, *1*, 245-276.
24. Davis, J.M.; Eder, B.K.; Nychka, D.; Yang, Q. Modeling the Effects of Meteorology on Ozone in Houston Using Cluster Analysis and Generalized Additive Models; *Atmos. Environ.* **1998**, *32*, 2505-2520.
25. *Korea Meteorological Administration Numerical Weather Prediction Division Technical Report*; KMA-2002-3, 2002.
26. Seaman, N.L.; Stauffer, D.R.; Lario-Gibbs, A.L. A Multiscale Four-Dimensional Data Assimilation System Applied in the San Joaquin Valley during SARMAP. Part I: Modeling Design and Basic Performance Characteristics; *J. Appl. Meteorol.* **1995**, *34*, 1739-1761.
27. Helmis, C.G.; Papadopoulos, K.H.; Kalogiros, J.A.; Soilemes, A.T.; Asimakopoulos, D.N. Influence of Background Flow on Evolution of Saronic Gulf Sea Breeze; *Atmos. Environ.* **1995**, *29*, 3689-3701.
28. Klemm, O.; Ziomas, I.C.; Balis, D.; Suppan, P.; Slemr, J.; Romero, R.; Vyras, L.G. A Summer Air-Pollution Study in Athens, Greece; *Atmos. Environ.* **1998**, *32*, 2071-2087.
29. Lu, R.; Turco, R.P. Ozone Distributions over the Los Angeles Basin: Three-Dimensional Simulations with the SMOG Model; *Atmos. Environ.* **1996**, *30*, 4155-4176.
30. Park, I.-S.; Lee, S.-J.; Kim, C.-H.; Yoo, C.; Lee, Y.-H. Simulating Urban-Scale Air Pollutants and their Predicting Capabilities over the Seoul Metropolitan Area; *J. Air & Waste Manage. Assoc.* **2004**, *54*, 695-710.
31. Arritt, R.W. Effects of the Large-Scale Flow on Characteristic Features of the Sea Breeze; *J. Appl. Meteorol.* **1993**, *32*, 116-125.
32. Tov, D.A.; Peleg, M.; Matveev, V.; Mahrer, Y.; Seter, I.; Luria, M. Recirculation of Polluted Air Masses over the East Mediterranean Coast; *Atmos. Environ.* **1997**, *31*, 1441-1448.
33. Zhang, S.; Takle, E. The Effects of Large-Scale Winds on the Sea-Land-Breeze Circulations in an Area of Complex Coastal Heating; *J. Appl. Meteorol.* **1993**, *32*, 1181-1195.
34. Kim, Y.-K.; Lee, H.W.; Oh, I.-B.; Jung, W.-S.; Song, S.-K.; Lim, Y.-K.; Hwang, M.-K. Vertical Ozone Distributions over the Seoul Metropolitan Area in June. In *Proceeding of the 36th Meeting of Korean Society for Atmospheric Environment*. Korean Society for Atmospheric Environment, Seoul, 2003; pp 113-114.
35. Sanchez-Coyllo, O.R.; Ynoue, R.Y.; Martins, L.D.; Andrade, M.F. Impacts of Ozone Precursor Limitation and Meteorological Variables on Ozone Concentration in Sao Paulo, Brazil; *Atmos. Environ.* **2006**, *40*, 552-562.
36. MacDonald, C.P.; Roberts, P.T.; Main. H.H.; Dye, T.S.; Coe, D.L.; Yarbrough, J. The 1996 Paso del Norte Ozone Study: Analysis of Meteorological and Air Quality Data That Influence Local Ozone Concentrations; *Sci. Total Environ.* **2001**, *276*, 93-109.
37. Hurley, P.J.; Manins, P.C. Meteorological Modeling on High-Ozone Days in Perth, Western Australia; *J. Appl. Meteorol.* **1995**, *34*, 1643-1652.

About the Authors
Mi-Kyoung Hwang, Yoo-Keun Kim, Hwa Woon Lee, and Cheol-Hee Kim are with the Division of Earth Environmental System, Busan National University, Busan, South Korea. In-Bo Oh is with the Institute for Multi-Dimensional Air Quality Studies, University of Houston, Houston, TX. Please address correspondence to: Yoo-Keun Kim, Busan National University, Busan, South Korea; phone: +82-51-515-1689; e-mail: kimyk@pusan.ac.kr.